American Mineralogist, Volume 95, pages 260–272, 2010

Chopinite-sarcopside solid solution, $[(Mg,Fe)_3\square](PO_4)_2$, in GRA95209, a transitional acapulcoite: Implications for phosphate genesis in meteorites

Edward S. Grew,[1,*] Martin G. Yates,[1] Rachel J. Beane,[2] Christine Floss,[3] and Christopher Gerbi[1]

[1]Department of Earth Sciences, University of Maine, 5790 Bryand Global Sciences Center, Orono, Maine 04469-5790, U.S.A.
[2]Geology Department, 6800 College Station, Bowdoin College, Brunswick, Maine 04011, U.S.A.
[3]Laboratory for Space Sciences and Physics Department, Washington University, CB1105, 1 Brookings Drive, St. Louis, Missouri 63130, U.S.A.

Abstract

Orthophosphate, $(Mg,Fe,Mn)_3(PO_4)_2$ with X_{Mg} = Mg/(Mg+Fe) = 0–0.89 and Mn/Fe = 0.05–0.3 and chladniite-johnsomervilleite, $MnNa_8(Ca_4Na_4)(Mg,Fe,Mn)_{43}(PO_4)_{36}$ with X_{Mg} = 0.44–0.81 and Mn/Fe = 0.3–0.8, are minor constituents of meteorite Graves Nunataks (GRA) 95209, a transitional acapulcoite consisting mostly of forsterite (Fa_7) and enstatite ($Wo_3Fs_{7–8}$) with subordinate clinopyroxene ($Wo_{41–45}Fs_{4–6}$) and plagioclase ($Or_{1–2}An_{10–19}$), and cut by Fe,Ni metal veins. Electron backscatter diffraction patterns and maps, together with chemical analyses and Fe-Mg-Mn distribution among phosphates, confirm identification of the orthophosphate as sarcopside, chopinite, and farringtonite; no graftonite was found. Phosphates are found as (1) narrow rims between metal and forsterite or orthopyroxene; (2) aggregates having the same outline as metal; and (3) inclusions and stringers in metal, including a ring around a graphite rosette. Electron microprobe analyses of sarcopside/chopinite-johnsomervilleite/chladniite pairs give a regular Fe-Mg distribution with $K_D = (Mg/Fe)_{Src/Chp}/(Mg/Fe)_{Jhn/Cld} = 0.584$ consistent with terrestrial sarcopside-johnsomervilleite pairs, whereas analyses of farringtonite-chladniite pairs give $K_D = 1.51$, but the Mg-Fe distribution is less regular. Textural relations suggest that Fe-Mn sarcopside originally formed by oxidation of P in metal and replacement of the metal and, through interaction with silicates, was converted to magnesian sarcopside-chopinite and farringtonite, i.e., the silicate matrix acted as a reservoir of Mg that could be exchanged with Fe and Mn in the sarcopside. Using the farringtonite-chopinite univariant curve determined in hydrothermal experiments by F. Brunet and others, isopleths calculated for the most magnesian chopinite in GRA95209, X_{Mg} = 0.65, give 4–7 kbar at 500–1100 °C, pressures far too high for the acapulcoite-lodranite parent body. Two scenarios could explain the discrepancy: (1) chopinite and magnesian sarcopside persisted metastably into the farringtonite stability field as Mg-Fe exchange progressed and the source volume for GRA95209 cooled; (2) a very mild shock event was intense enough to convert Fe-rich farringtonite (X_{Fe} = 0.4–0.6) to magnesian sarcopside and chopinite, but not enough to deform olivine in the source volume. Whether metastability could have played a role in chopinite formation would best be answered by experiments on the $Mg_3(PO_4)_2$–$Fe_3(PO_4)_2$ system under anhydrous conditions. If the transformation was found to be as kinetically fast as in the hydrothermal experiments, then shock would become the more plausible explanation for the presence of chopinite in this meteorite.

Keywords: Meteorite, phosphate, electron microprobe, electron backscatter diffraction, chopinite, sarcopside, chladniite, achondrite

Introduction

Three ferromagnesian phosphate minerals with the stoichiometry $(Mg,Fe^{2+},Mn,Ca)_3(PO_4)_2$ (orthophosphate) and Fe or Mg > (Mn+Ca) have been found in meteorites (Fig. 1). Graftonite and sarcopside, which are Fe-dominant, are characteristic of iron meteorites (e.g., Olsen and Fredriksson 1966; Olsen et al. 1999; Sugiura and Hoshino 2003), whereas the Mg-dominant farringtonite is characteristic of pallasites (e.g., DuFresne and Roy 1961; Buseck and Holdsworth 1977). A second Mg-dominant mineral, chopinite (Grew et al. 2007), which is isostructural with sarcopside, was recently found in a granulite facies paragneiss in East Antarctica. Experiments in the $Mg_3(PO_4)_2$ system show that chopinite is a high-pressure analog of farringtonite (Brunet and Vielzeuf 1996; Brunet et al. 1998). The discovery of chopinite is consistent with experimental evidence for complete solid solution between end-member chopinite $Mg_3(PO_4)_2$ and end-member sarcopside $Fe_3^{2+}(PO_4)_2$ (e.g., Annersten and Nord 1980; Charalampides et al. 1988). Farringtonite containing as little as 40% $Mg_3(PO_4)_2$ has been synthesized (Annersten et al. 1980), whereas no more than 20% $Mg_3(PO_4)_2$ has been reported in synthetic graftonite (Nord and Ericsson 1982b).

GRA95209 is a primitive achondrite, i.e., a stony meteorite lacking chondrules (near-spherical silicate objects generally 100 μm to a few millimeters across), but with mineral assemblages and chemical compositions characteristic of chondritic meteorites. It consists mostly of forsterite (Fa_7) and enstatite ($Wo_3Fs_{7–8}$),

* E-mail: esgrew@maine.edu

0003-004X/10/0203–260$05.00/DOI: 10.2138/am.2010.3153

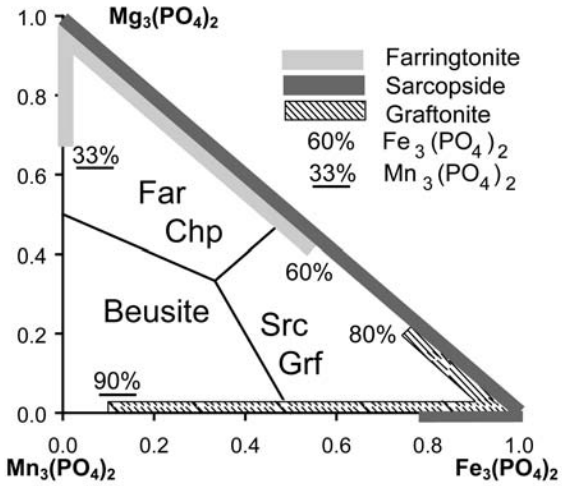

FIGURE 1. Maximum binary ranges in mol% $Fe_3(PO_4)_2$ and $Mn_3(PO_4)_2$ for compositions of $(Mg,Fe,Mn)_3(PO_4)_2$ (orthophosphate) structures obtained by synthesis. Farringtonite at 1 bar, 800 °C (Annersten et al. 1980; Nord and Stefanidis 1980), Mn-Fe sarcopside at 200–800 bars, 300 °C (Ericsson et al. 1986), Mg-Fe sarcopside at 500–800 bars, 300–650 °C (Charalampides et al. 1988), Fe-Mg chopinite at 30 kbar, 600 °C (Annersten and Nord 1980), and graftonite at 1 bar, 800 °C (Nord and Ericsson 1982a, 1982b). Fields for individual minerals: Far = farringtonite, Chp = chopinite, Grf = graftonite, Src = sarcopside.

with subordinate clinopyroxene ($Wo_{41–45}Fs_{4–6}$) and plagioclase ($Or_2An_{17–19}$), and is cut by Fe,Ni metal veins (McBride and Mason 1997; Mittlefehldt and Lindstrom 1998; McCoy et al. 2006; this study). It was originally classed as a lodranite (McBride and Mason 1997), but more recent studies suggest it is better considered a transitional acapulcoite because of siderophile element abundances indicative of Fe-FeS cotectic melting and, compared to the lodranites, relatively high rare-earth element contents in the silicate minerals attributable to limited silicate melting (Mittlefehldt and Lindstrom 1998; Floss 2000; Patzer et al. 2004). Both types of meteorites are believed to have originated from a single parent asteroid that experienced extensive Fe,Ni metal-FeS cotectic melting and variable silicate melting (McCoy et al. 1996, 1997a, 1997b). The temperature for melting in the case of GRA95209 is bracketed by the Fe-FeS cotectic at 950 °C and incipient silicate melting at 1050 °C. Pressure estimates are much less well constrained because the size of the parent body is difficult to estimate. Cooling rates give a radius of less than 10 km for the parent body if the meteorites originated from the core; more likely, the body was several tens of kilometers in radius, but not more than 100 km (McCoy et al. 1997b). For a parent body of 100 km radius and average density 3.6 g/cm^3, lithostatic pressure at the center would not exceed 200 bars (Dodd 1981).

The phosphates chladniite, whitlockite, and orthophosphate, $(Mg,Fe^{2+},Mn)_3(PO_4)_2$, are minor phases in GRA95209 (McCoy and Carlson 1998; Floss 1999; McCoy et al. 2006). Six published electron microprobe analyses of orthophosphate gave Mg/(Mg+Fe) ratios (X_{Mg}) ranging from 0.80–0.87 ("farringtonite," McCoy et al. 2006) through 0.44–0.58 ("Mg-graftonite," Floss 1999) to 0.01 ("graftonite/sarcopside," McCoy et al. 2006), all containing subordinate Mn and negligible Ca. In principle, given the low pressures estimated for formation of this meteorite, all the reported compositions except the most Fe-rich should be farringtonite, but previous studies have not been able to confirm the identification of the orthophosphates.

After the discovery of the relatively high-pressure mineral chopinite [$Mg_3(PO_4)_2$-II of Brunet and Vielzeuf 1996; Brunet et al. 1998] in a crustal rock formed at 6–7 kbar, we decided to re-examine the orthophosphates in GRA95209 and identify them using electron backscatter diffraction, a non-destructive method applicable to top-polished petrographic sections. We studied the three polished thin sections (PTS) in which Floss (1999) and McCoy et al. (2006) reported ferromagnesian phosphate: PTS ,39 and ,40 of the matrix and the polished section PS ,150 from a metal-rich sheet in matrix. New electron microprobe analyses of these phases give a nearly continuous range in X_{Mg} from 0.89 to 0.01. However, electron backscattered diffraction diagrams and the distributions of Fe, Mn, and Mg between orthophosphate and associated chladniite suggest that three orthophosphates are present: farringtonite (X_{Mg} = 0.80–0.87) and chopinite-sarcopside (X_{Mg} = 0.65–0.01). These findings resulted in a conundrum: how could a relatively high-pressure phase be stable in an asteroid in which lithostatic pressures were but a few hundred bars?

MINERAL IDENTIFICATION USING ELECTRON BACKSCATTERED DIFFRACTION

Electron backscatter diffraction (EBSD) was applied to distinguish the orthophosphates, which cannot be identified on composition alone. Back-scattered electrons emitted from a specimen in a scanning electron microscope (SEM) form a diffraction pattern that is imaged on a phosphor screen. Analysis of the diffraction pattern allows crystallographic phase identification after accounting for chemical composition (Prior et al. 1999). The EBSD studies were conducted at Bowdoin College on a LEO 1450VP SEM outfitted with an HKL Nordlys II detector and Channel 5 software (software details in Schmidt and Olesen 1989). The sample was prepared by taking a standard polished thin section and polishing approximately six additional hours in a non-crystallizing colloidal silica suspension on vibratory polisher (SYTON method of Fynn and Powell 1979). The thin section was not carbon coated; charging was minimized by using a chamber pressure of 14 Pa, combined with the 70° tilt required for pattern acquisition. EBSD patterns were collected in interactive mode and in automated mapping mode. Operating parameters for collecting EBSD patterns were an accelerating voltage of 20 kV, a working distance of 25 mm, and a beam current of 2.2 nA. Channel 5 acquisition and indexing settings were 4 × 4 binning, high gain, Hough resolution = 65, 7 bands, and 80 reflectors. Indexing the acquired EBSD patterns requires a match unit to be created from known crystallographic parameters using a kinematic electron diffraction model (Schmidt and Olesen 1989; Prior et al. 1999). For this project, match units were produced for graftonite (Calvo 1968), sarcopside (Moore 1972), chopinite (Grew et al. 2007), and farringtonite (Nord and Kierkegaard 1968). During data processing, accepted data were limited to those points with mean angular deviation (MAD) less than 1° based on the number of bands (7) detected and experimental work of Krieger Lassen (1996) on the precision of crystal orientations.

Good matches were obtained in both interactive (e.g., Fig. 2) and mapping modes (Table 1) for sarcopside, chopinite, and farringtonite in PTS ,40 and PS ,150, and maps yielded a farringtonite distribution consistent with the back-scattered electron (BSE) image (Fig. 3). In automatic mapping mode, most graftonite solutions were rejected based on their high MAD (>1); the graftonite solutions also are mostly isolated points or "patchwork" with other solutions, further supporting the decision to reject the indexing of these points. Furthermore, no good matches were found for graftonite in the interactive mode, even for nearly Mg-free compositions [Mg/(Mg+Fe) = 0.01 in PS ,150, see below], and we thus conclude this phase is absent in the three sections.

Because the thin section slice was beginning to peel off the glass, PTS ,39 could not be polished sufficiently well for EBSD work, and no suitable patterns could be obtained on this section. Identification of grains not analyzed by EBSD in PTS ,39 and ,40 was based on similarity in composition to grains analyzed by EBSD, contrast in back-scattered electron images and/or element distributions, whereas similarity in composition was the sole criterion for identifying grains analyzed in PS ,150 by McCoy et al. (2006), including unpublished data (McCoy personal communication 2005). One grain reported by McCoy (personal communication 2005) gave a composition intermediate

Table 1. Statistics for automatic mapping using electron backscattered diffraction of areas 1 and 4 of polished thin section GRA 95209 ,40

	Chopinite	Sarcopside	Farringtonite	Graftonite
		1-2a		
no. of points	1206	1185	136	251
mean MAD	0.89 ± 0.21	0.84 ± 0.21	1.21 ± 0.18	1.16 ± 0.10
MADmin	0.32	0.29	0.71	0.68
mean BC	128	130	96	100
Interpretation	present	present	absent	absent
		1-2b		
no. of points	208	333	50	48
mean MAD	0.68 ± 0.29	0.68 ± 0.25	1.18 ± 0.20	1.20 ± 0.19
MADmin	0.25	0.24	0.76	0.71
mean BC	121	122	95	94
Interpretation	present	present	absent	absent
		4-1		
no. of points	93	46	219*	109
mean MAD	1.18 ± 0.19	1.18 ± 0.20	0.65 ± 0.33	1.10 ± 0.20
MADmin	0.64	0.72	0.19	0.70
mean BC	91	76	101	88
Interpretation	absent	absent	present	absent

Note: MAD = Mean angular deviations; BC = band contrast. Criterion for determining whether a mineral is present: MAD < 1.
* See Figure 3c.

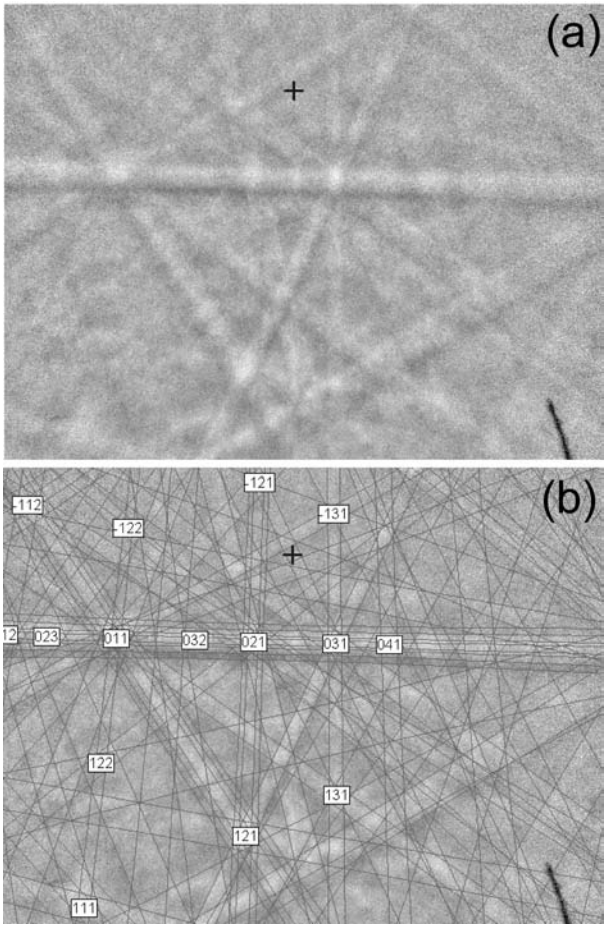

Figure 2. (**a**) Kikuchi pattern for chopinite section PTS ,40, area 1-2b. The numbers on the image are Miller indices for the poles at the intersection of the bands, which are produced by specific sets of crystallographic planes. The mean angular deviations for the match (**b**) are 0.536. The + in both images is an artifact of the calibration (basically pattern centering).

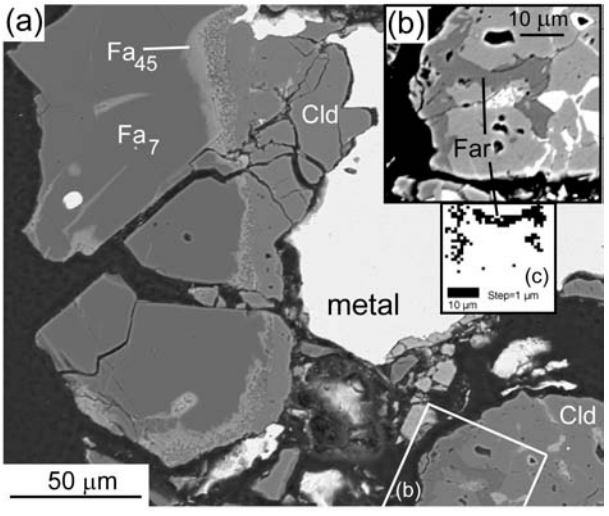

Figure 3. Back-scattered electron (BSE) images of fayalitic rims on forsterite in GRA95209, PTS ,40, area 4 (Table 2). Speckled band between fayalitic rim and chladniite is a mixture of fayalitic olivine and silica (identification using energy dispersive spectroscopy). Dark areas are epoxy exposed by fragmentation of the section. (**b**) Contrast-enhanced, brightened, and enlarged portion of BSE image enclosed in white frame in **a** to bring out M-shaped area of farringtonite (Table 6). (**c**) Map of the M-shaped area of farringtonite obtained by electron backscatter diffraction (Table 1 for area 4-1) using only points with MAD < 1 (all farringtonite, pixels plotted as black squares). The white area of the map includes pixels from matches with MAD > 1 (Table 1) and pixels for which no match could be found among the phases listed in Table 1. Cld = chladniite, Fa = fayalite content of forsterite (in mole percent from electron microprobe analysis), Far = farringtonite.

between farringtonite and chopinite, the only case too equivocal to identify confidently.

Phosphate microstructures

In transmitted light, the orthophosphates are largely opaque, whereas chladniite is more commonly transparent (Fig. 4). In PTS ,39 and ,40, aggregates of the orthophosphates have the same outlines as the Fe,Ni metal, so only the slivers and rims of chladniite serve to distinguish them from metal at low magnification in plane polarized light. As a result BSE images were much more useful for distinguishing the phosphates to study textural relations in these two sections, whereas in PS ,150 BSE images are the only means. On the basis of EBSD of selected grains, we found that phosphate appearing darker (lower scattering) is farringtonite (e.g., Fig. 3), whereas phosphate appearing lighter is sarcopside-chopinite or johnsomervilleite-chladniite; these two series could easily be distinguished with energy dispersive spectroscopy (EDS).

Phosphates are found as (1) narrow rims between metal and forsterite or orthopyroxene; (2) aggregates; and (3) inclusions and stringers in metal. The rims consist of chladniite and minor farringtonite, and have a highly irregular outline (Figs. 5a and 5b). The aggregates are complex intergrowths of chopinite-sarcopside, chladniite-johnsomervilleite, and subordinate farringtonite (Figs. 5c–5f); only rarely is farringtonite present with chopinite (Fig. 5e). In general, highly pitted areas of sarcopside-chopinite are surrounded by rims of johnsomervilleite-chladniite with less pitted surfaces, e.g., an oval dominated by chladniite surrounds sarcopside in which pitting lends a streaky or wavy appearance (Fig. 5d). The phosphates embay metal and, in places, enclose metal particles, which could be contributing to their opacity. However, fine-grained graphite could also be contributing to the opacity. Pits in phosphate give more C counts from the electron beam than smooth surfaces, although not as many counts as the larger graphite masses, a few of which are enclosed in chladniite (Fig. 5d). Chladniite and minor farringtonite are included in metal in PTS ,39 and ,40 and a small amount of chopinite-sarcopside is found in one inclusion in PTS ,40. In contrast, phosphate enclosed in metal at the margin of the metal sheet or in matrix adjacent to the metal sheet in PS ,150 is commonly sarcopside, either in rounded masses (Fig. 6a), stringers (McCoy et al. 2006) or, in one case, a complete ring around a graphite nodule (Fig. 6b). Contiguous minerals include Fe,Ni metal and Fe,Ni phosphide, which McCoy et al. (2006) identified as kamacite and schreibersite, respectively.

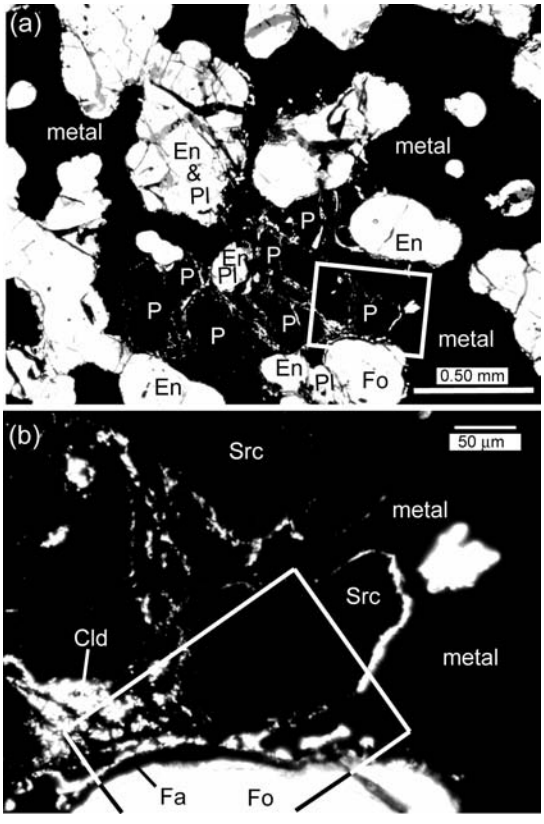

Figure 4. Photomicrographs of GRA95209 PTS ,39, area 1 in transmitted plane polarized light showing relation of phosphate (P), largely sarcopside, to Fe,Ni metal (cf. Floss 1999, Fig. 1a). Rectangle in **a** indicates location of **b**; rectangle in **b** corresponds roughly to Figure 5c. Cld = chladniite, En = enstatite, Fa = fayalite, Fo = forsterite, Pl = plagioclase, Src = sarcopside.

Enstatite, forsterite, plagioclase, and less commonly, diopside are found in the vicinity of the phosphate. Forsterite in contact with phosphate is distinctly enriched in Fe in opaque rims (Figs. 4b and 5c); patches of fayalite are found among phosphate, forsterite, and enstatite (Fig. 5f). The transition from unaltered forsterite to Fe-enriched rim is relatively abrupt overall, but is intricate in detail (Fig. 3a).

Chemical composition

Phosphates and silicates were analyzed with a Cameca SX-100 electron microprobe (EMP) at the University of Maine using wavelength dispersive analysis. Analytical conditions were 15 kV accelerating voltage, 10 nA beam current, and the data were processed using the X-Phi correction of Merlet (1994). A focused beam was used for phosphates, a 5 µm beam for silicates. The phosphate data were calibrated with albite (Na$K\alpha$, Al$K\alpha$), diopside (Mg$K\alpha$, Si$K\alpha$, Ca$K\alpha$), fluorapatite (P$K\alpha$), sanidine (K$K\alpha$), rutile (Ti$K\alpha$), synthetic Cr_2O_3 (Cr$K\alpha$), rhodonite (Mn$K\alpha$), almandine (Fe$K\alpha$), and pentlandite (Ni$K\alpha$); the silicate data, with several different sets of mineral and synthetic standards.

With a few exceptions, oligoclase, enstatite, and forsterite are remarkably constant in composition in the three sections studied (Tables 2–4), and our major and most minor element compositions agree with those reported in these and other sections (Mittlefehldt and Lindstrom 1998; McCoy et al. 2006); an exception is the diopside Cr content, which is somewhat higher in the two grains we analyzed. Oligoclase is mostly $Or_{1–2}An_{17–18}$, but one grain and a zone in another are more sodic: An_{10}. The Fe-enriched rims on forsterite are also enriched in Mn and give low totals, 97.6–99.7 wt%. Their composition varies within a rim and from one rim to another, e.g., Si = 0.974–1.015 per 4 O (cf. Si = 0.994–1.005 atoms in forsterite) and X_{Mg} [=Mg/(Mg+Fe)] = 0.22–0.55 (e.g., Table 2). Individual analyses give up to 1 wt% P_2O_5, which could be due to very fine phosphate impurities.

In the three sections studied here (Table 5; Fig. 7), chladniite-

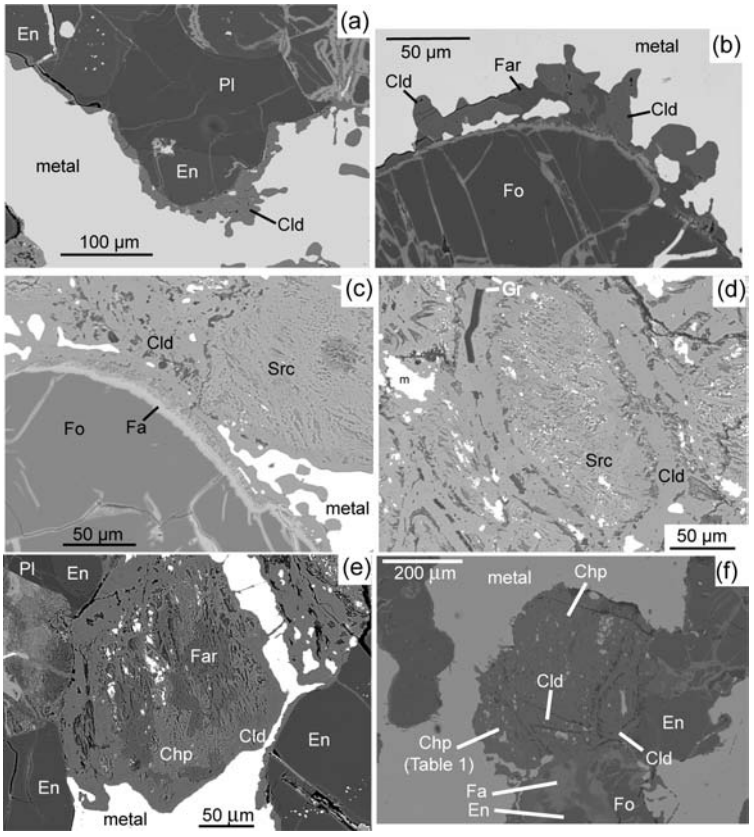

◀**Figure 5.** Back-scattered electron images of phosphates in GRA95209. (**a**) Chladniite rim between metal and plagioclase plus enstatite, PTS ,39, area 1-8. (**b**) Chladniite and farringtonite in rim near forsterite, PTS ,39, area 5 (**c**) Forsterite with fayalite rim against chladniite and sarcopside, PTS ,39, area 1-3 (cf. rectangle in Fig. 4b). (**d**) Sarcopside with pitted surface surrounded by rim of chladniite, containing plates of graphite, PTS ,39, area 1-4. (**e**) Three-phase phosphate assemblage, PTS ,39, area 2-1. (**f**) Chopinite (confirmed with EBSD, Table 1, analysis Table 6) and chladniite; unmarked area is a mixture, PTS ,40, area 1. Note patch of fayalite between enstatite and forsterite. Chp = chopinite, Cld = chladniite, En = enstatite, Fa = fayalite, Far = farringtonite, Fo = forsterite, Gr = graphite, Src = sarcopside.

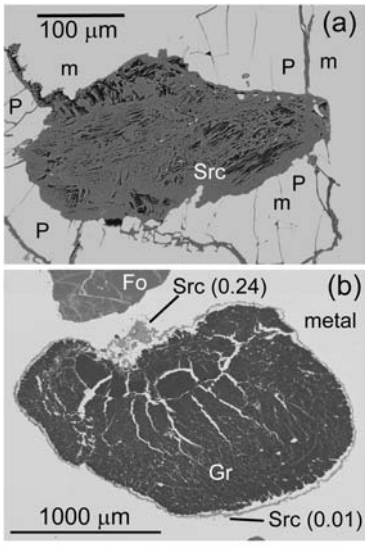

Figure 6. Back-scattered electron images of phosphates in GRA95209, PS ,150. (**a**) Sarcopside (confirmed with EBSD) surrounded by Fe,Ni metal (m) and Fe,Ni phosphide (P), area 3 in matrix near the metal-rich sheet. To illustrate details in sarcopside microstructure, contrast between metal and phosphide had to be sacrificed because both are so much brighter than sarcopside. (**b**) Sarcopside ring (confirmed with EBSD) in metal around a large graphite rosette at the edge of the metal-rich sheet; there are also tiny graphite specks between the ring and the rosette. The maximum (Table 6) and minimum X_{Mg} = Mg/(Mg+Fe) in the ring are given in parentheses (also Fig. 8b). Fo = forsterite, Gr = graphite, Src = sarcopside.

johnsomervilleite solid solutions range in X_{Mg} from 0.81 to 0.44, but even more magnesian chladniite was reported in PTS ,210, where whitlockite is also found (McCoy et al. 2006). The Mn/Fe ratio decreases markedly with increasing X_{Mg} (Fig. 8a). An average of formulae calculated for 144 O from our data gives P = 36.06 ± 0.12, total Mn+Mg+Fe+Ni = 44.08 ± 0.34 (Fig. 9a), Na+K = 11.84 ± 0.16, and Ca = 3.69 ± 0.29 (Fig. 9b), a close approximation to an ideal formula $MnNa_8(Ca_4Na_4)(Mg,Fe,Mn)_{43}(PO_4)_{36}$. That is, most of the variation from grain to grain in GRA95209 (Figs. 7 and 9a) is accommodated at the Mg1–9 and Fe10 sites (site notation of Grew et al. 2006), while Ca and Na contents at the Na1, X, Ca1, and Ca2 sites remain relatively constant. Moreover, Mn could occupy the (0,0,0) site in GRA95209 chladniite as it does in fillowite, ideally $MnNa_8(Ca_4Na_4)Mn_{43}(PO_4)_{36}$, whereas Ca was presumed to occupy the (0,0,0) site in type chladniite (Grew et al. 2006).

Compositions of the orthophosphates (Table 6) show a trend very similar to chladniite (Fig. 10), whereas the range of Mn/Fe ratios is less (Fig. 8b). A few farringtonite grains are weakly zoned, most notably no. 6 in PTS ,39: X_{Mg} = 0.80–0.84. Overall, farringtonite in GRA95209 is less magnesian than that reported heretofore, X_{Mg} = 0.80–0.89 (a possible farringtonite grain with X_{Mg} = 0.73 is queried as its identity could not be confirmed) vs. 0.89–0.97 in pallasites and one IIE iron (Fuchs et al. 1973; Bild 1974; Buseck and Holdsworth 1977), though well within the 0.4–1.0 range of synthetic $Mg_3(PO_4)_2$ with the farringtonite structure (Fig. 1 from Annersten et al. 1980). As reported by McCoy et al. (2006), the most Fe-rich sarcopside is found in the metal-rich sheet either as stringers or as a ring around a graphite rosette (Fig. 6b).

Sarcopside in GRA95209 is far more magnesian than that previously reported in meteorites. Buseck and Holdsworth (1977) reported an unidentified phase approximating the $(Fe^{2+},Mg)_3(PO_4)_2$ stoichiometry that could be sarcopside with X_{Mg} = 0.12–0.23 in the Brahin pallasite, but sarcopside has only been confirmed in IIIAB and IVA irons, where it is Mg-free (Bild 1974; Olsen et al. 1999). In summary, the presence of both farringtonite and chopinite-sarcopside in a single meteorite is

TABLE 2. Selected average analyses of olivine

Mineral	forsterite	fayalite	forsterite	forsterite	fayalite	forsterite	forsterite	forsterite	fayalite
Section/grain	39/1-3	39/1-3 rim	39/2-1	40/1-1	40/1-1 rim	40/4-2	40/4-2 rim	150/2-1	150/2-1rim
No.	10	9	10	15	9	10	6	14	12
					wt%				
SiO_2	41.62	31.32	41.76	41.65	32.28	41.63	35.67	41.59	31.86
TiO_2	0.03	0.03	0.00	0.02	0.00	0.00	0.03	0.00	0.02
Al_2O_3	0.01	0.00	0.00	0.03	0.00	0.03	0.01	0.02	0.00
Cr_2O_3	0.05	0.02	0.03	0.04	0.03	0.02	0.00	0.00	0.00
MgO	51.55	9.70	51.26	51.66	11.57	52.00	25.38	51.72	12.47
MnO	0.52	3.66	0.55	0.54	3.77	0.55	1.13	0.56	4.08
FeO	6.73	52.74	6.93	7.01	50.37	6.93	37.38	7.08	49.79
NiO	0.05	0.04	0.00	0.05	0.00	0.04	0.04	0.01	0.05
CaO	0.02	0.01	0.02	0.02	0.01	0.03	0.05	0.03	0.01
Na_2O	0.01	0.01	0.00	0.00	0.00	0.01	0.00	0.01	0.02
K_2O	0.00	0.00	0.00	0.00	0.00	0.00	0.01	0.00	0.00
P_2O_5	0.01	0.11	0.00	0.02	0.01	0.01	0.03	0.00	0.19
Total	100.59	97.65	100.55	101.04	98.05	101.24	99.72	101.01	98.50
					Formulae per 4 O				
Si	1.001	1.005	1.005	0.998	1.015	0.996	1.008	0.998	0.996
Ti	0.001	0.001	0.000	0.000	0.000	0.000	0.001	0.000	0.000
Al	0.000	0.000	0.000	0.001	0.000	0.001	0.000	0.001	0.000
Cr	0.001	0.000	0.001	0.001	0.001	0.000	0.000	0.000	0.000
Mg	1.848	0.464	1.838	1.846	0.542	1.854	1.069	1.850	0.581
Mn	0.011	0.099	0.011	0.011	0.100	0.011	0.027	0.011	0.108
Fe	0.135	1.415	0.139	0.140	1.324	0.139	0.883	0.142	1.302
Ni	0.001	0.001	0.000	0.001	0.000	0.001	0.001	0.000	0.001
Ca	0.001	0.001	0.001	0.000	0.000	0.001	0.001	0.001	0.000
Na	0.000	0.001	0.000	0.000	0.000	0.000	0.000	0.000	0.001
K	0.000	0.000	0.000	0.000	0.000	0.000	0.000	0.000	0.000
P	0.000	0.003	0.000	0.001	0.000	0.000	0.001	0.000	0.005
Total	2.998	2.990	2.995	3.000	2.984	3.003	2.991	3.002	2.996
X_{Mg}	0.932	0.247	0.930	0.929	0.290	0.930	0.548	0.929	0.309
Figure reference	5c	5c	5e*	5f	5f	3a	3a	–	–

Notes: No. = number of individual analyses in the average. All Fe as FeO. X_{Mg} = Mg/(Mg+Fe).
* Fo in 39/2-1 is just outside the field of view.

TABLE 3. Selected average analyses of pyroxene

Mineral	enstatite	enstatite	enstatite	diopside
Section/grain	39/2-1a	40/1-1	150/2-1	150/2-1
No.	10	10	15	15
		wt%		
SiO_2	57.59	58.48	57.37	54.40
TiO_2	0.24	0.17	0.21	0.68
Al_2O_3	0.33	0.34	0.34	0.72
Cr_2O_3	0.67	0.76	0.72	2.21
MgO	34.59	34.46	34.45	17.54
MnO	0.61	0.62	0.64	0.30
FeO	4.73	4.71	5.16	2.03
NiO	0.00	0.07	0.00	0.01
CaO	1.51	1.60	1.67	21.43
Na_2O	0.08	0.09	0.08	1.14
K_2O	0.00	0.00	0.00	0.00
P_2O_5	0.01	0.00	0.01	0.00
Total	100.36	101.30	100.66	100.47
		Formulae per 6 O		
Si	1.978	1.989	1.971	1.967
Ti	0.006	0.004	0.005	0.019
Al	0.013	0.013	0.014	0.031
Cr	0.018	0.020	0.020	0.063
Mg	1.771	1.747	1.765	0.946
Mn	0.018	0.018	0.019	0.009
Fe	0.136	0.134	0.148	0.062
Ni	0.000	0.002	0.000	0.000
Ca	0.056	0.058	0.061	0.830
Na	0.005	0.006	0.005	0.080
K	0.000	0.000	0.000	0.000
P	0.000	0.000	0.000	0.000
Total	4.002	3.993	4.009	4.007
X_{Mg}	0.929	0.929	0.923	0.939
Figure reference	5e	5f	–	–

Notes: No. = number of individual analyses in the average. All Fe as FeO. X_{Mg} = Mg/(Mg+Fe).

TABLE 4. Selected average analyses of plagioclase

Section/grain	39/2-1	39/1-8	40/5	150/2-1
No.	10	10	6	15
		wt%		
SiO_2	63.65	63.51	63.95	63.54
TiO_2	0.08	0.05	0.05	0.05
Al_2O_3	22.71	22.85	22.63	22.71
Cr_2O_3	0.00	0.00	0.00	0.00
MgO	0.00	0.01	0.01	0.01
MnO	0.02	0.01	0.04	0.01
FeO	0.20	0.20	0.52	0.38
NiO	0.00	0.00	0.01	0.00
CaO	3.71	3.80	3.59	3.73
Na_2O	9.31	9.34	9.46	9.37
K_2O	0.24	0.25	0.24	0.31
P_2O_5	0.01	0.00	0.01	0.01
Total	99.93	100.02	100.52	100.12
		Formulae per 8 O		
Si	2.814	2.808	2.816	2.809
Ti	0.003	0.002	0.002	0.002
Al	1.184	1.191	1.175	1.184
Cr	0.000	0.000	0.000	0.000
Mg	0.000	0.001	0.001	0.001
Mn	0.001	0.000	0.001	0.000
Fe	0.007	0.007	0.019	0.014
Ni	0.000	0.000	0.000	0.000
Ca	0.176	0.180	0.169	0.176
Na	0.798	0.801	0.808	0.804
K	0.014	0.014	0.013	0.017
P	0.000	0.000	0.000	0.000
Total	4.996	5.003	5.005	5.007
Ab	80.8	80.5	81.6	80.6
Or	1.4	1.4	1.4	1.7
An	17.8	18.1	17.1	17.7
Figure reference	5e	5a	–	–

Notes: No. = number of individual analyses in the average. All Fe as FeO.

TABLE 5. Selected average analyses of chladniite and johnsomervilleite

Mineral	Cld	Cld	Cld	Cld	Cld	Cld	Jhm
Section/grain	39/2-1	39/1-3	39/1-8	39/5	40/2-3	40/4-1	150/2-1
No.	15	15	10	13	15	15	11
				wt%			
P_2O_5	47.33	45.26	46.45	47.91	48.29	48.66	43.48
SiO_2	0.01	0.03	0.06	0.03	0.04	0.04	0.01
TiO_2	0.00	0.02	0.01	0.00	0.03	0.00	0.00
Al_2O_3	0.02	0.00	0.03	0.08	0.04	0.00	0.03
Cr_2O_3	0.03	0.04	0.02	0.00	0.02	0.05	0.08
MgO	20.47	13.86	18.37	22.64	22.46	24.05	9.59
CaO	4.16	3.28	3.75	4.11	4.14	4.30	3.04
MnO	8.32	13.12	9.76	7.09	7.12	6.16	16.65
FeO	12.94	17.76	15.34	11.67	11.91	10.15	21.32
NiO	0.08	0.04	0.07	0.00	0.07	0.00	0.04
Na_2O	6.62	6.42	6.68	6.80	6.87	6.92	6.45
K_2O	0.01	0.00	0.00	0.00	0.00	0.01	0.01
Total	100.00	99.83	100.54	100.32	100.99	100.35	100.71
				Formulae per 144 O			
P	36.151	36.222	35.943	36.028	36.106	36.168	35.819
Si	0.011	0.027	0.054	0.027	0.036	0.034	0.008
Ti	0.000	0.016	0.009	0.000	0.022	0.000	0.000
Al	0.024	0.001	0.028	0.086	0.042	0.000	0.038
Cr	0.020	0.032	0.017	0.000	0.013	0.033	0.065
Mg	27.535	19.528	25.026	29.983	29.565	31.479	13.906
Ca	4.025	3.317	3.672	3.909	3.915	4.050	3.172
Mn	6.357	10.508	7.556	5.331	5.326	4.582	13.723
Fe	9.764	14.037	11.725	8.668	8.795	7.452	17.354
Ni	0.060	0.029	0.050	0.000	0.052	0.000	0.035
Na	11.585	11.776	11.845	11.709	11.765	11.785	12.172
K	0.006	0.005	0.000	0.000	0.000	0.012	0.009
Total	95.537	95.498	95.924	95.742	95.638	95.595	96.301
X_{Mg}	0.738	0.582	0.681	0.776	0.771	0.809	0.445
Figure reference	5e	5c	5a	5b	–	3a*	–

Notes: No. = number of individual analyses in the average. All Fe as FeO. X_{Mg} = Mg/(Mg+Fe).
* Near to analyzed farringtonite in Figure 3b.

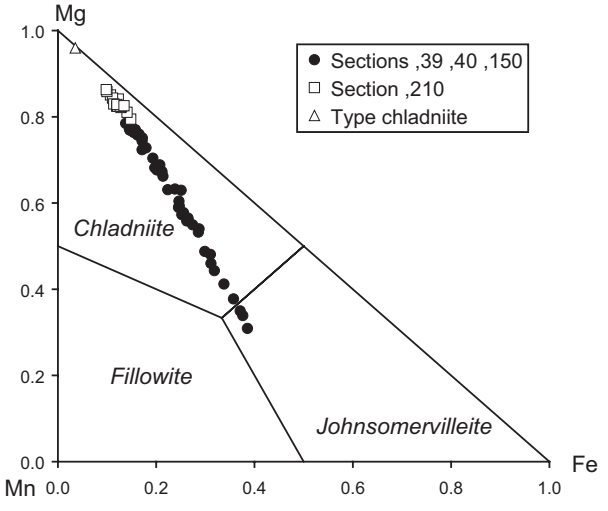

FIGURE 7. Plot of chladniite and johnsomervilleite composition in terms of the major components. Sources of data: GRA95209 (four sections) = Floss (1999); T. McCoy (personal communication 2005); McCoy et al. (2006); this study. Type (Carlton IIICD) = McCoy et al. (1994).

unique to GRA95209; and the wide range of Fe/Mg ratios in sarcopside has not been previously reported in any single occurrence, whether meteoritic or terrestrial. Mg-poor sarcopside in area 6 of PS ,150 (X_{Mg} = 0.01–0.02, Fig. 6b) has a higher X_{Mn} = Mn/(Mn+Fe) = 0.23 than the sarcopside richest in Mn in the

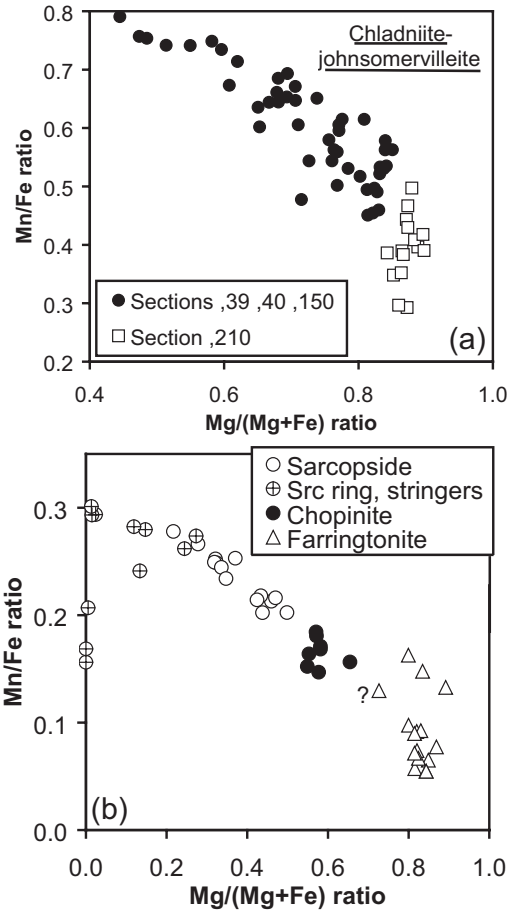

FIGURE 8. (**a**) Variation of Mn/Fe ratio with X_{Mg} = Mg/(Mg+Fe) ratio in chladniite-johnsomervilleite. (**b**) Variation of Mn/Fe ratio with X_{Mg} = Mg/(Mg+Fe) ratio in orthophosphates in PTS ,39 and ,40 and PS ,150. Ring and stringers of sarcopside (Src) occur in the metal sheet in PS ,150 (e.g., Fig. 6b). The identity of one composition (queried farringtonite) is richer in Fe than other farringtonite. Sources of data: Floss (1999); T. McCoy (personal communication 2005); McCoy et al. (2006); this study.

IIIAB and IVA irons (X_{Mn} = 0.04, Olsen et al. 1999).

Nickel contents of the silicates are uniformly low, whereas Ni tends to increase with Fe content in farringtonite and chladniite-johnsomervilleite, reaching 0.11 and 0.23 wt% NiO, respectively. Chopinite-sarcopside NiO content ranges more widely, reaching 0.65 wt% in sarcopside, and show no obvious trend, e.g., the sarcopside richest in Fe in PS ,150 (e.g., Fig. 6b) contains relatively little NiO (0.03–0.08 wt%, e.g., grain 6-4, Table 6, except one grain giving 0.39 wt%). Fractionation of Ni and Fe among the phosphates is not regular. It is possible that submicroscopic metal particles could be contributing to the Ni content as well as to the opacity of the orthophosphates.

DISTRIBUTION OF MG, FE, AND MN

In selecting locations for analysis, we sought spots on the phosphates and silicates as close together as possible with the objective of measuring distribution coefficients between the various minerals.

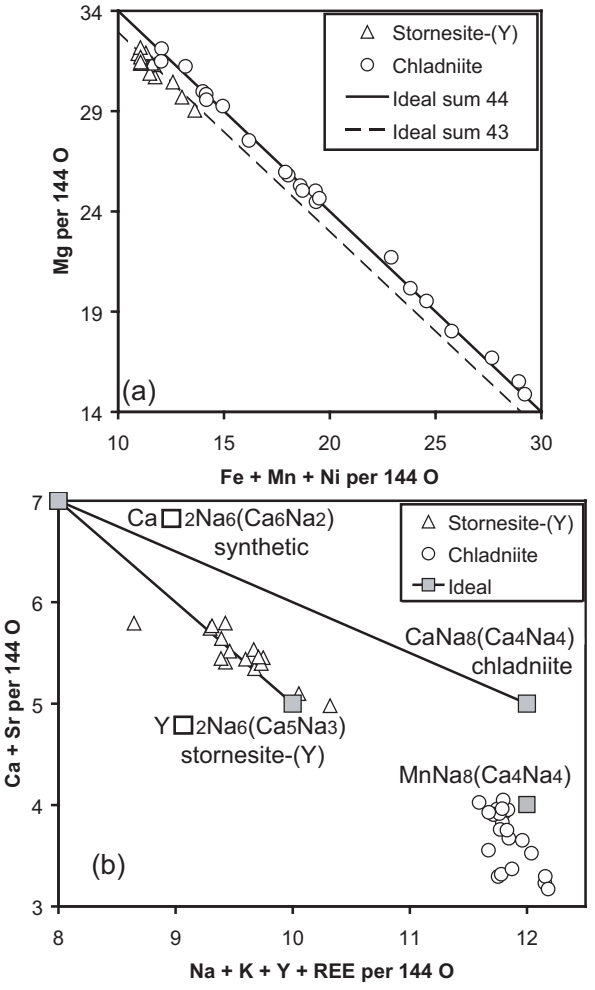

FIGURE 9. Plots of chladniite (GRA95209 only) and stornesite-(Y) compositions in terms of divalent cations excluding Ca (**a**) and in terms of Ca, Na, K, and Y (+REE) (**b**). Stornesite-(Y) data are from Grew et al. (2006); K and Ni were not analyzed. Only data from U. Maine Cameca SX100 are included. Formulae for ideal members are based on Grew et al. (2006) for (0,0,0), Na1, X, Ca1, and Ca2 sites.

Although the silicates (excluding the fayalitic rims on forsterite) have a constant composition in all the areas studied, the phosphates vary extensively in both Mg/Fe and Mn/Fe ratios, and there is no evidence for an equilibrium Fe-Mg distribution between the phosphates and silicates (Table 7). The distribution coefficients, $K_D = (Mg/Fe)_{silicate}/(Mg/Fe)_{phosphate}$, are at least an order of magnitude higher in GRA95209 than comparable K_D measured on pairs that more likely approached equilibrium: (1) forsterite ($Fa_{7.0}$) and type chladniite, which occur together in a silicate-bearing inclusion in the Carlton IIIAB iron (McCoy et al. 1994), and (2) forsterite coexisting with farringtonite in the Springwater pallasite (Olsen and Fredriksson 1966). The K_D for enstatite-chopinite was estimated from chopinite associated with biotite in one thin section from the type sample of chopinite and from biotite associated with enstatite in another section from the type (Grew et al. 2007). That is, the phosphates in GRA95209 are considerably more Fe-rich than they should be had they equilibrated with the main mass of silicate. In contrast, a least-squares fit to six pairs of chladniite and fayalitic olivine, mostly in rims (e.g., Figs. 3a and 5c) gives a K_D much closer to the possible equilibrium pair (0.28 vs. 0.49, Table 7), which could be interpreted to indicate a closer approach to the equilibrium distribution between olivine and chladniite at a very local scale with little involvement of the main mass of Mg-rich silicate.

In contrast, there is much greater regularity in the distribution of Mg, Fe, and Mn among the phosphates. The most regular is the distribution of Mg and Fe between chopinite-sarcopside and chladniite, for which the distribution coefficient, $K_D = (Mg/Fe)_{Src\text{-}Chp}/(Mg/Fe)_{Cld}$, is 0.584, which is nearly identical to the Mg-Fe distribution between terrestrial sarcopside and johnsomervilleite, $K_D = 0.588$ (Grew et al. 2007), but differs from the distribution between terrestrial graftonite and johnsomervilleite, $K_D = 0.276$ (Fig. 11a). The distribution between farringtonite and chladniite is much less regular (Fig. 11b). Figure 11 gives a $K_D = (Mg/Fe)_{Far}/(Mg/Fe)_{Src\text{-}Chp} = 2.589$ from the least-square fits for sarcopside-chopinite and farringtonite relative to chladniite, higher than $K_D = 2.100$ calculated from the three-phase assemblage in Figure 5e and $K_D = 2.28$–2.30 estimated by Grew et al. (2007), partly on the basis of the farringtonite and chladniite compositions reported by McCoy et al. (2006). Figure 11 shows that chladniite Mg/Fe ratios are greatest in assemblages with farringtonite and least in assemblages with chopinite-sarcopside and intermediate in assemblages with both farringtonite and chopinite. This relationship, together with the regular distribution, is consistent with approach to an equilibrium Fe-Mg distribution. Approach to equilibrium could have been facilitated by accommodation of Mg and Fe only at the Mg1–9 and Fe10 sites with negligible involvement of other sites in chladniite (see above). Distribution of Mn and Fe between sarcopside-chopinite, and chladniite in GRA95209 is reasonably regular and is much closer to the Mn-Fe distribution between sarcopside and johnsomervilleite than to that between graftonite and johnsomervilleite in terrestrial occurrences and IIIAB iron meteorites (Fig. 12). However, extrapolations of the trends for sarcopside-chopinite and farringtonite in GRA95209 are not aimed at the origin, which is the case for the terrestrial occurrences and IIIAB iron meteorites, but intersect the abscissa at Mn/Fe ≈ 0.5 in chladniite, a clear indication of non-equilibrium. Distribution of Mn could have been affected by its presence at the (0,0,0) site as well as at the Mg1–9 and Fe10 sites in chladniite.

PRESSURE-TEMPERATURE CONDITIONS

Pressure-temperature evolution of GRA95209

Meteorite GRA95209 underwent extensive melting of an Fe,Ni metal and FeS component while part of the acapulcoite and lodranite parent body (McCoy et al. 2006). This indicates the meteorite experienced temperatures of $T > 950$ °C, the metal-sulfide cotectic. Evidence for extensive silicate melting or loss of silicate melts is equivocal and localized, i.e., temperatures would have not exceeded 1050 °C. The extent of melting is one reason GRA95209 was reclassified as a transitional acapulcoite; it differs both from lodranites, in which silicate melting had been extensive and temperatures reached ~1150–1200 °C, and

TABLE 6. Selected average analyses of orthophosphate, $(Mg,Fe)_3(PO_4)_2$

Mineral	Chp	Chp	Chp	Src	Src	Src	Src	Far	Far	Far	Far
Section/grain	39/2-1	40/1-1	39/2-2	39/1-3	39/1-5b	150/3-1	150/6-4	39/2-1	39/5	40/2-3	40/4-1
No.	13	16	13	9	5	8	10	14	12	11	3
						wt%					
P_2O_5	47.49	45.98	46.41	44.84	43.13	42.01	40.06	50.11	51.53	50.89	52.41
SiO_2	0.02	0.02	0.03	0.02	0.08	0.00	0.02	0.02	0.01	0.04	0.02
TiO_2	0.00	0.00	0.03	0.00	0.06	0.00	0.00	0.00	0.03	0.02	0.02
Al_2O_3	0.01	0.02	0.02	0.03	0.02	0.01	0.04	0.02	0.02	0.00	0.02
Cr_2O_3	0.00	0.00	0.00	0.01	0.04	0.00	0.00	0.01	0.01	0.00	0.00
MgO	25.10	20.93	20.75	15.60	11.18	6.29	0.39	32.68	36.96	35.41	38.70
CaO	0.01	0.01	0.01	0.01	0.04	0.02	0.02	0.02	0.03	0.01	0.05
MnO	3.64	4.98	5.06	6.87	8.65	11.12	13.30	2.35	0.75	1.18	1.10
FeO	23.58	27.94	27.82	32.66	37.44	40.55	45.94	14.62	11.73	12.91	8.36
NiO	0.16	0.26	0.15	0.24	0.14	0.35	0.04	0.11	0.02	0.09	0.02
Na_2O	0.03	0.00	0.00	0.00	0.00	0.02	0.04	0.02	0.03	0.03	0.00
K_2O	0.01	0.00	0.00	0.00	0.03	0.00	0.00	0.01	0.00	0.00	0.00
Total	100.04	100.14	100.28	100.29	100.81	100.37	99.84	99.98	101.12	100.57	100.69
						Formulae per 8 O					
P	1.998	1.991	2.002	2.003	1.986	2.004	2.006	2.006	1.997	1.998	2.009
Si	0.001	0.001	0.001	0.001	0.004	0.000	0.001	0.001	0.001	0.002	0.001
Ti	0.000	0.000	0.001	0.000	0.002	0.000	0.000	0.000	0.001	0.001	0.001
Al	0.000	0.001	0.001	0.002	0.002	0.001	0.003	0.001	0.001	0.000	0.001
Cr	0.000	0.000	0.000	0.000	0.002	0.000	0.000	0.000	0.000	0.000	0.000
Mg	1.860	1.596	1.576	1.227	0.906	0.529	0.034	2.303	2.522	2.448	2.612
Ca	0.000	0.000	0.001	0.001	0.002	0.001	0.001	0.001	0.001	0.000	0.002
Mn	0.153	0.216	0.219	0.307	0.398	0.531	0.666	0.094	0.029	0.046	0.042
Fe	0.980	1.195	1.186	1.442	1.703	1.911	2.272	0.578	0.449	0.501	0.317
Ni	0.006	0.011	0.006	0.010	0.006	0.016	0.002	0.004	0.001	0.004	0.001
Na	0.003	0.000	0.000	0.000	0.000	0.002	0.005	0.002	0.003	0.003	0.000
K	0.000	0.000	0.000	0.000	0.002	0.000	0.000	0.001	0.000	0.000	0.000
Total	5.003	5.012	4.994	4.993	5.014	4.994	4.991	4.991	5.005	5.002	4.985
X_{Mg}	0.655	0.572	0.571	0.460	0.347	0.217	0.015	0.799	0.849	0.830	0.892
X_{Mn}	0.135	0.153	0.156	0.176	0.190	0.217	0.227	0.140	0.061	0.085	0.117
Figure reference	5e	5f	–	5c	–	6a	6b	5e	5b	–	3b, 3c
EBSD	–	Chp	–	–	–	Src	Src	–	–	Far	Far

Notes: No. = number of individual analyses in the average. All Fe as FeO. X_{Mg} = Mg/(Mg+Fe); X_{Mn} = Mn/(Mn + Fe). EBSD = identification using electron backscattered diffraction; chopinite (Chp) is distinguished from sarcopside (Src) on basis of chemistry; Far = farringtonite.

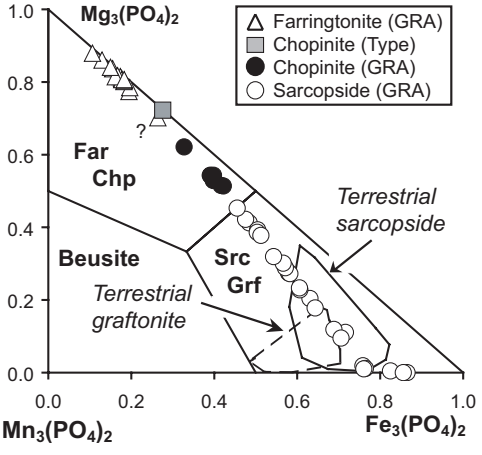

FIGURE 10. Compositions (mole proportions) of $(Mg,Fe,Mn)_3(PO_4)_2$ phases analyzed in the three sections of GRA95209 (Floss 1999; McCoy personal communication 2005; McCoy et al. 2006; this study). Identity of the phases is based on electron backscattered diffraction or on being close in composition to grains so characterized. However, the identity of one composition (queried farringtonite) is richer in Fe than other farringtonite. Data for type chopinite and terrestrial compositions are from Grew et al. (2007) supplemented by analyses of sarcopside and graftonite in a sample from the Bull Moose Mine, South Dakota (this study), Loch Quoich, Scotland (F. Hatert personal communication 2007), and Cyrilov, Czech Republic (Škoda et al. 2007). Fields for individual minerals: Far = farringtonite, Chp = chopinite, Grf = graftonite, Src = sarcopside.

TABLE 7. Distribution coefficients (K_D) between silicate and phosphate in GRA95209 and comparison with other areas

	K_D*	K_D†	K_D‡
$(Mg/Fe)_{Ol}/(Mg/Fe)_{Cld}$	3.1	0.28	0.49
$(Mg/Fe)_{Fo}/(Mg/Fe)_{Far}$	1.6	–	0.24
$(Mg/Fe)_{En}/(Mg/Fe)_{Chp}$	6.7	–	~0.8

* From averages of forsterite and enstatite (Tables 2 and 3) with most magnesian chladniite, farringtonite, and chopinite (Tables 5 and 6).
† Six pairs of chladniite and fayalitic olivine in GRA95209, $R^2 = 0.74$.
‡ Sources given in the text.

acapulcoites, in which silicates did not melt and temperatures were ~950–1000 °C (McCoy et al. 1996, 1997a; Mittelfehldt and Lindstrom 1998; Floss 2000; Patzer et al. 2004). Moreover, McCoy et al. (2006) suggested that the metal sheet cutting the meteorite (and present in PS ,150) could have formed at ~1200 °C elsewhere in the parent body and was later intruded into the part from which GRA95209 originated, where the temperature was ~1000 °C, a suggestion consistent with heating of the parent body being localized and variable (Mittlefehldt et al. 1996). Because it originated from a higher temperature area, the metal sheet would be more reduced than the matrix.

Using various methods, investigators have deduced dramatically different scenarios for the cooling history of the acapulcoite-lodranite parent body. Pellas et al. (1997) calculated a relatively rapid cooling rate of 100 ± 40 K/Ma from 1030 to 450 °C followed by slow cooling of 1.7–3.7 K/Ma to 190 °C for the Acapulco meteorite, whereas Zipfel et al. (1995) inferred a period a slow cooling followed cooling of 100 K/Ma at 900 °C

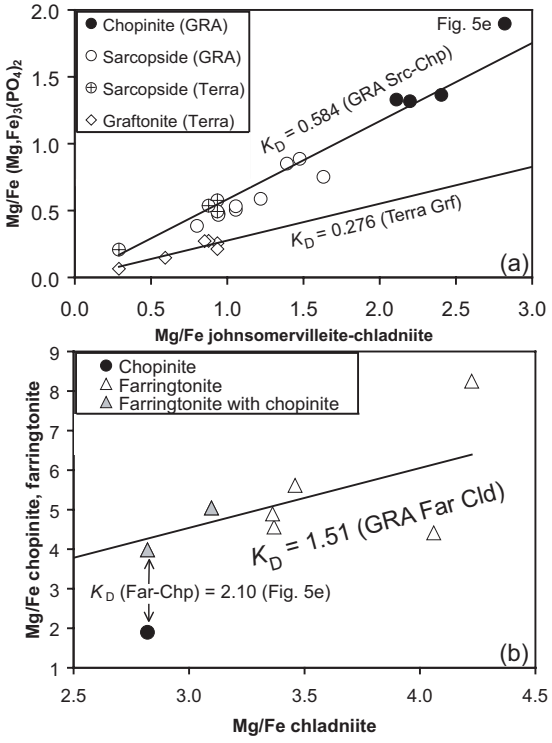

FIGURE 11. Mg/Fe ratios of coexisting chladniite and sarcopside-chopinite in GRA95209 (GRA) and terrestrial (Terra) occurrences (**a**) and between chladniite and farringtonite in GRA95209 (**b**). (**a**) K_D = $(Mg/Fe)_{Src}/(Mg/Fe)_{Cld}$; R^2 = 0.936 for least-squares fit to sarcopside-chopinite (GRA95209 data only) and K_D = $(Mg/Fe)_{Grf}/(Mg/Fe)_{Cld}$; R^2 = 0.858 for least-squares fit to terrestrial graftonite. (**b**) The two points give K_D (Far-Chp) = $(Mg/Fe)_{Far}/(Mg/Fe)_{Chp}$ from analytical data on grains analyzed in PTS ,39 area 2-1 (Fig. 5e) and the line gives a least-squares fit for all the farringtonite data: K_D = $(Mg/Fe)_{Far}/(Mg/Fe)_{Cld}$; R^2 = 0.411. Chopinite in the second 3-phase assemblage did not give a satisfactory analysis, and so is not plotted. Sources for terrestrial pairs: Corbella i Cordomí and Malgarejo i Draper (1990), Černý et al. (1998), Livingstone (1980), Roda et al. (2004), F. Hatert (personal communication 2007); for GRA95209 (this study).

and preceded fast cooling at 650 °C for this meteorite. For lodranites, McCoy et al. (1997a) estimated relatively slow cooling of 1–100 K/Ma above 1000 °C and much more rapid cooling from 1000 to 400 °C.

It is unlikely that lithostatic pressures exceeded more than a few hundred bars given the maximum radius of 100 km estimated for the parent body, but absence of shock effects such as undulatory extinction in olivine (McCoy et al. 2006) only constrains shock pressures to be less than 40 kbar (Stöffler et al. 1991). Very weak shock effects (S2 stage of Stöffler et al. 1991) are reported from a few other acapulcoites (McCoy et al. 1996), whereas a few lodranites show shock effects reaching the S3 and S4 stages (McCoy et al. 1997a).

Decay of ^{26}Al and ^{60}Fe is the most plausible source of heat for the high temperatures experienced by acapulcoites and lodranites in the early stage of evolution, although impacts could have resulted in heating events during later stages (Zipfel et al. 1995; McCoy et al. 1996; Pellas et al. 1997; Lee 2008).

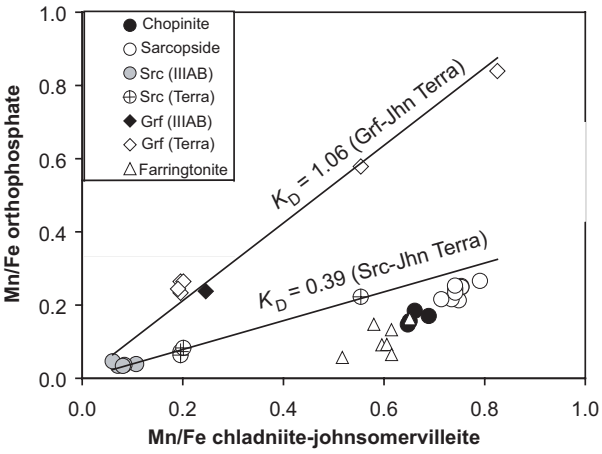

FIGURE 12. Mn/Fe ratios of coexisting chladniite-johnsomervilleite (Jhn), sarcopside (Src)-chopinite, graftonite (Grf) and farringtonite in GRA95209 (this study), terrestrial occurrences (Terra; sources are given in caption for Fig. 11) and IIIAB iron meteorites (Olsen et al. 1999). Lines are least-squares fit to terrestrial graftonite-johnsomervilleite pairs (R^2 = 0.969) and terrestrial sarcopside-johnsomervilleite pairs (R^2 = 0.986).

Sarcopside/graftonite relationships

Beginning with Olsen and Fredriksson (1966), most investigators have thought that graftonite is the high-temperature polymorph of $Fe_3(PO_4)_2$, and specific temperatures for the sarcopside-graftonite transition, 740–750 °C, have been cited (Modaressi et al. 1983; Kaell et al. 1984), but the source of this information was not given. To date the polymorphic transition has been studied only by synthesis experiments, which lend support to graftonite being the higher-temperature polymorph. Korinth and Royen (1961) reported synthesis of graftonite by reduction of Fe^{3+}-bearing phosphates over a wide range of temperatures (500–950 °C), a process used by Kostiner and Rea (1974) to synthesize graftonite at 800 °C. Trömel and Schwerdtfeger (1963) identified as graftonite the $Fe_3(PO_4)_2$ phase formed between 940 and 1020 °C, mostly in association with Fe-phosphate melt and Fe metal. In contrast, sarcopside synthesis has been successful only under hydrothermal conditions at pressures exceeding atmospheric, e.g., Mattievich and Danon (1977) synthesized sarcopside at 300 °C and 0.8 kbar. Other authors synthesized end-member sarcopside by hydrothermally treating graftonite or other compounds in the Fe-P-O system at 300–586 °C and 0.8–3.0 kbar pressure (Ericsson et al. 1986; Charalampides et al. 1988; Warner et al. 1992; Schmid-Beurmann 2001). However, a major role for pressure seems unlikely because the polymorphs have nearly identical cell volumes (Schmid-Beurmann 2001). Indeed, graftonite has a slightly smaller cell volume per formula unit than sarcopside, viz. 150.4(1) vs. 150.7(1) Å^3 (Kostiner and Rea 1974; Nord and Ericsson 1982a; Ericsson et al. 1986), and thus one would expect that graftonite should be the higher-pressure phase. Schmid-Beurmann (2001) ruled out a role for metastability in synthesizing sarcopside, but there is too little information to justify this conclusion.

Syntheses show graftonite is the preferred host for Mn, whereas sarcopside is the preferred host for Mg (Fig. 1). Compo-

sitional ranges of natural sarcopside and graftonite are consistent with the ranges determined from syntheses along the binaries except that Mn in sarcopside can exceed the limit implied by the Mn-Fe binary (Fig. 10). However, the very presence of sarcopside in GRA95209 and other meteorites is not consistent with the reported syntheses. Mn-bearing sarcopside would not be expected to be the stable polymorph at the temperatures and pressures inferred for GRA95209, particularly as the fractionation of Mn into graftonite (Figs. 10 and 12) should stabilize graftonite to lower temperature. In addition, the difference in cell volume increases with increasing Mn content (calculated from cell parameters reported by Nord and Ericsson 1982a and Ericsson et al. 1986), suggesting that in Mn-bearing systems, sarcopside should be favored by decreasing pressure.

It would be possible to reconcile meteoritic occurrences of sarcopside with available syntheses and cell-volume data if graftonite synthesis is assumed to be metastable and conversion to sarcopside under hydrothermal conditions the result of more favorable kinetics, i.e., sarcopside is the stable phase at the pressures and temperatures of the experiments. This conclusion is consistent with the presence of sarcopside rich in Mn and poor in Mg in GRA95209 (Fig. 6b; Table 6) that formed at T = 950–1050 °C and P < 1 kbar. It is also consistent with sarcopside formation in the IIIAB irons as proposed by Olsen et al. (1999), who concluded that sarcopside was the first phosphate to form, in a few cases as a liquidus phase, and during cooling sarcopside partially recrystallized to graftonite. However, the presence of graftonite remains unexplained, particularly a graftonite (identity confirmed by X-ray diffraction) with X_{Mn} = 0.02 in the View Hill IIIA iron described by Olsen et al. (1999).

Terrestrial occurrences offer little insight because of the additional complexity resulting from the (1) widespread occurrence of sarcopside and graftonite in lamellar intergrowths with each other and other phosphates; (2) presence of Ca and other constituents; and (3) relatively elevated pressures of formation. Possibly the contradictions could be resolved with reversed experiments of the polymorphic transition.

Chopinite/farringtonite relationships

Chopinite (isostructural with sarcopside) and farringtonite are polymorphs of $Mg_3(PO_4)_2$, and the polymorphic transition is well characterized by reversed experiments that demonstrate chopinite is stabilized at relatively high pressures and low temperatures (Brunet and Vielzeuf 1996; Brunet et al. 1998, reproduced in Fig. 13). Synthetic farringtonite can incorporate significant amounts of Mn and Fe (Fig. 1) and, thus, Fe-Mg orthophosphate with >40% $Mg_3(PO_4)_2$ is expected to be farringtonite in meteorites. However, identification of chopinite was confirmed for orthophosphate with 57% $Mg_3(PO_4)_2$ by EBSD, and for orthophosphate with 65% $Mg_3(PO_4)_2$ by association with even more magnesian orthophosphate (Fig. 5e) and by its Mg-Fe distribution (Fig. 11). Chopinite with these compositions would not have been stable at the pressures indicated for GRA95209. For example, calculations for the chopinite-farringtonite-chladniite assemblage in PTS ,39 area 2-1 (Fig. 5e) give pressures from 4 kbar at 500 °C to 7 kbar at 1100 °C, assuming both solid solutions are ideal and using either the K_D = 2.100 determined for this assemblage or the K_D = 2.589 from all the analyses considered together (Figs. 11 and 13). Assuming K_D = 6.2, the minimum implicit in the synthesis of sarcopside with 40% $Mg_3(PO_4)_2$ at 0.8 kbar, 500 °C (Charalampides et al. 1988), stabilization of chopinite with 65% $Mg_3(PO_4)_2$ requires 5 kbar at 950 °C. In summary, stabilization of chopinite at P < 1 kbar and 950 °C does not seem possible even if non-ideality in the chopinite and farringtonite solid solutions also played a role in lowering the pressure.

Origin of the phosphate assemblages

The origin of ferromagnesian phosphates in meteorites has puzzled scientists for some time, and GRA95209 is no exception. Olsen and Frederiksson (1966) proposed that sarcopside and graftonite formed in iron and pallasite meteorites from subsolidus oxidation of phosphide associated with Fe,Ni metal or of P contained in the metal. In a much larger study involving detailed study of phosphate assemblages in IIIAB iron meteorites, Olsen et al. (1999) further proposed the involvement of sulfide melt, which would have been a source of Mn for the phosphate. Floss (1999) proposed an analogous scenario for the formation of "Mg-graftonite" (sarcopside-chopinite) involving oxidation of P in the Fe,Ni metal or phosphide and exchange of Fe for Mg with silicates during thermal metamorphism of GRA 95209, and further suggested that chladniite formed later by reaction of sarcopside-chopinite with plagioclase or directly from Fe,Ni metal by a process involving oxidation and exchange of Fe for Mg, Na, and Ca in the silicate matrix. McCoy et al (2006) contrasted the more oxidized matrix where phosphate coexisted with tetrataenite with the more reduced metal sheet where Fe-Ni phosphide (schreibersite) was present; kamacite+graphite are present in both assemblages.

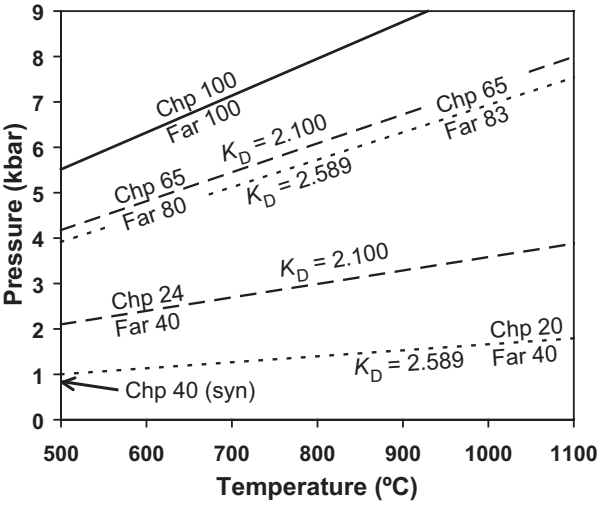

Figure 13. Isopleths calculated from the experimentally determined reaction and volume change in the $Mg_3(PO_4)_2$ system (solid line) for end-member chopinite and farringtonite (Brunet and Vielzeuf 1996; Brunet et al. 1998) assuming ideal solid solution for both minerals (Grew et al. 2006, 2007). The K_D values are taken from the analytical data on PTS ,39 area 2-1 and the least-squares fits in Figure 11 (dashed and dotted lines, respectively). Chp 65 and Far 80 are measured composition [in terms of 100 Mg/(Mg+Fe) atomic]; the other values are calculated. Charalampides et al. (1988) synthesized sarcopside with 40% $Mg_3(PO_4)_2$ at 0.8 kbar, 500 °C (arrow).

Textural relations are consistent with the suggestion that the larger phosphate aggregates in GRA95209 resulted from oxidation of P in Fe,Ni metal and replacement of the metal, i.e., the aggregates have the same outline as the metal (e.g., Fig. 4a) and phosphates embay metal and enclose metal particles (Figs. 5c–5f). NiO contents of sarcopside-chopinite (Table 6) on average exceed those of forsterite and enstatite (Tables 2–3), which is consistent with the phosphate resulting from oxidation of Fe,Ni metal as Floss (1999) noted; some NiO could be contributed by metal particles too fine to see in the BSE images. The graphite rosettes could have served as loci for oxidation: the ring of sarcopside in Figure 6b can be interpreted as an example illustrating the beginning of the replacement process in which oxidation of P gives Mg-free phosphate in the vicinity of a rosette at the margin of the metal sheet. An advanced stage is the oval of sarcopside surrounded by chladniite (Fig. 5d) that could be outlining a former rosette that the band and fine particles of graphite are relics of; indeed the orthophosphates may owe their opacity more to finely dispersed graphite particles than to particles of metal. This interpretation implies that the metal sheet (or at least its margin) approached the oxidation state of the matrix after its intrusion (cf. McCoy et al. 2006), consistent with equilibration of trace elements in metal reported by Herrin et al. (2006). Moreover, a shreibersite-sarcopside assemblage (Fig. 6a) in the matrix adjacent to the sheet suggests that shreibersite and phosphate could have formed at the same oxygen fugacity, further evidence that sheet metal (or its margin) and matrix metal had equilibrated.

In the IIIAB iron meteorites sarcopside, graftonite, and johnsomervilleite remained free of Mg, whereas in GRA95209, which contains abundant forsterite and enstatite, interaction of phosphates with silicates resulted in exchange of Fe, Mg, and Mn between the two, i.e., the silicate matrix acted as a reservoir of Mg that could be exchanged with Fe in the phosphate, driving phosphate compositions almost to the Mg end-members with little change in silicate composition. End-member sarcopside is far out of chemical equilibrium with olivine and pyroxene containing 92–93% of the Mg end-members; the distribution should be much closer, cf. $(Mg/Fe)_{En}/(Mg/Fe)_{Chp}$ estimated to be about 0.8 for type chopinite (Table 7). The presence of Mg-bearing sarcopside ($X_{Mg} = 0.24$) in the ring in Figure 6b implies exchange at an early stage of oxidation, i.e., Mg-Fe exchange proceeded coevally with oxidation of phosphorus. Mn/Fe ratios decrease with increasing X_{Mg} (Fig. 7) in most cases, suggesting exhaustion of the Mn source, most likely troilite, as the exchange progressed. The differences in Mn/Fe ratios between Mg-poor sarcopside in the ring and stringers (upper and lower trends in Fig. 8b) could be due to access to the troilite source. The fayalitic rims on forsterite (Figs. 3a, 4b, and 5c) could represent a later stage of the exchange when an equilibrium distribution of Fe and Mg between these rims and nearby chladniite was approached (Table 7) yet diffusion of Fe, Mg, and Mn within olivine was limited to these rims.

Most surprising is that exchange of Mg for Fe occurred under conditions where the Mg-substituted sarcopside containing 40% or more of the $Mg_3(PO_4)_2$ component did not invert to farringtonite as expected from experimental evidence for stability of farringtonite in this compositional range (Fig. 1). Because the Mg-Fe distribution among the phosphates shows some equilibrium features, one scenario is that equilibrium might have been approached, but that it was metastable: chopinite and magnesian sarcopside persisted metastably into the farringtonite stability field as Mg-Fe exchange progressed and the source volume for GRA95209 cooled. The microstructural relationship between farringtonite and chopinite illustrated in Figure 5e could be interpreted as the interior of a mass of metastable chopinite having inverted to the stable phase, farringtonite, leaving a margin of uninverted chopinite. A difficulty with this scenario is that the farringtonite-chopinite transformation was found to be kinetically fast under hydrothermal conditions, e.g., it went to completion in 13 h at 824 °C (Brunet and Vielzeuf 1996; Brunet et al. 1998). Thus, metastable persistence of chopinite does not seem plausible unless the reaction is greatly slowed at very low water activities.

An alternative scenario is that a very mild shock event was intense enough to convert Fe-rich farringtonite ($X_{Fe} = 0.4–0.6$) to magnesian sarcopside and chopinite, but not enough to deform olivine in the source volume. In this case, the microstructures in Figure 5e could be interpreted as pre-existing farringtonite having been partially converted to chopinite along the margin of the mass by an increase in pressure due to shock. This shock affected the source while it was still hot enough for Mg-Fe exchange to proceed. Evidence for shock is reported from other meteorites of the acapulcoite-lodranite parent body (McCoy et al. 1996, 1997a), but not in GRA95209. Thus, the phosphates could be registering shock too weak to affect traditional shock indicators in meteorites.

In summary, the question of whether metastability could have played a role in chopinite formation in GRA95209 would best be answered by experiments on the $Mg_3(PO_4)_2$–$Fe_3(PO_4)_2$ system under anhydrous conditions. If the transformation were still found to be kinetically fast, then shock would become the more plausible explanation for the presence of chopinite in this meteorite.

Acknowledgments

We thank Kevin Righter of NASA for the loan of three sections of GRA95209. We thank Tim McCoy for permission to include his unpublished analyses of chladniite, farringtonite, chopinite, and sarcopside (sections 40, 150, and 210 of GRA95209) in Figures 7, 8, 10, and Frédéric Hatert for permission to include his unpublished analyses of graftonite and johnsomervilleite from Loch Quoich (Scotland) in Figures 10, 11, and 12. Michael Roden and Takashi Mikouchi are thanked for their constructive reviews and Rhian Jones for editorial handling of the manuscript. The research of both E.S.G. and M.G.Y. was supported by U.S. National Science Foundation grants OPP-0228842 and MRI-0116235 to the University of Maine. SEM-EBSD analyses supported by NSF grants MRI-0320871 and CCLI-9951390 to R.J.B.

References cited

Annersten, H. and Nord, A.G. (1980) A high pressure phase of magnesium orthophosphate. Acta Chemica Scandinavica, A34, 389–390.

Annersten, H., Ericsson, T., and Nord, A.G. (1980) The cation ordering in iron-containing zinc and magnesium orthophosphates determined from Mössbauer spectroscopy. Journal of Physics and Chemistry of Solids, 41, 1235–1240.

Bild, R.W. (1974) New occurrences of phosphates in iron meteorites. Contributions to Mineralogy and Petrology, 45, 91–98.

Brunet, F. and Vielzeuf, D. (1996) The farringtonite/$Mg_3(PO_4)_2$-II transformation: A new curve for pressure calibration in piston-cylinder apparatus. European Journal of Mineralogy, 8, 349–354.

Brunet, F., Chopin, C., and Seifert, F. (1998) Phase relations in the MgO-P_2O_5-H_2O system and the stability of phosphoellenbergerite: Petrological implications. Contributions to Mineralogy and Petrology, 131, 54–70.

Buseck, P.R. and Holdsworth, E. (1977) Phosphate minerals in pallasite meteorites. Mineralogical Magazine, 41, 91–102.

Calvo, C. (1968) The crystal structure of graftonite. American Mineralogist, 53, 742–750.

Černý, P., Selway, J.B., Ercit, T.S., Breaks, F.W., Anderson, A.J., and Anderson, S.D. (1998) Graftonite-beusite in granitic pegmatites of the Superior Province: A study in contrasts. Canadian Mineralogist, 36, 367–376.

Charalampides, G., Ericsson, T., Nord, A.G., and Khangi, F. (1988) Studies of hydrothermally prepared $(Fe,M)_3(PO_4)_2$-sarcopsides. Neues Jahrbuch für Mineralogie Monatshefte, 324–336.

Corbella i Cordomí, M. and Melgarejo i Draper, J.-C. (1990) Características y distribución de los fosfatos de las pegmatitas graníticas de la península del Cap de Creus (Pirineo oriental catalán). Boletin de la Sociedad Española de Mineralogía, 13, 169–182.

Dodd, R.T. (1981) Meteorites. A Petrologic-Chemical Synthesis, 368 p. Cambridge University Press, U.K.

DuFresne, E.R. and Roy, S.K. (1961) A new phosphate mineral from the Springwater pallasite. Geochimica et Cosmochimica Acta, 24, 198–205.

Ericsson, T., Nord, A.G., and Åberg, G. (1986) Cation partitioning in hydrothermally prepared olivine-related (Fe,Mn)-sarcopsides. American Mineralogist, 71, 136–141.

Floss, C. (1999) Fe,Mg,Mn-bearing phosphates in the GRA95209 meteorite: Occurrences and mineral chemistry. American Mineralogist, 84, 1354–1359.

——— (2000) Complexities on the acapulcoite-lodranite parent body: Evidence from trace element distributions in silicate minerals. Meteoritics and Planetary Science, 35, 1073–1085.

Fuchs, L.H., Olsen, E., and Gebert, E. (1973) New X-ray and compositional data for farringtonite, $Mg_3(PO_4)_2$. American Mineralogist, 58, 949–951.

Fynn, G.W. and Powell, W.J.A. (1979) The Cutting and Polishing of Electro-optic Materials, 215 p. Adam Hilger, Bristol.

Grew, E.S., Armbruster, T., Medenbach, O., Yates, M.G., and Carson, C.J. (2006) Stornesite-(Y), $(Y, Ca)\square_2Na_6(Ca,Na)_8(Mg,Fe)_{43}(PO_4)_{36}$, the first terrestrial Mg-dominant member of the fillowite group, from granulite-facies paragneiss in the Larsemann Hills, Prydz Bay, East Antarctica. American Mineralogist, 91, 1412–1424.

——— (2007) Chopinite, $[(Mg,Fe)_3\square](PO_4)_2$, a new mineral isostructural with sarcopside, from a fluorapatite segregation in granulite-facies paragneiss, Larsemann Hills, Prydz Bay, East Antarctica. European Journal of Mineralogy, 19, 229–245.

Herrin, J.S., Mittelfehldt, D.W., and Humayun, M. (2006) History of metal veins in acapulcoite-lodranite clan meteorite GRA 95209. Meteoritics and Planetary Science, 41, supplement, A75 (abstract).

Kaell, J.C., Jeannot, F., and Gleitzer, C. (1984) Étude de la reduction ménagée de $Fe_3(PO_4)_2$ et $Fe_9(PO_4)O_8$. Annales de Chimie—Science des Matériaux, 9, 169–180.

Korinth, J. and Royen, P. (1961) Reaktionen im system $Fe_2O_3/FePO_4$. Zeitschrift für Anorganische und Allgemeine Chemie, 313, 121–137.

Kostiner, E. and Rea, J.R. (1974) Crystal structure of ferrous phosphate, $Fe_3(PO_4)_2$. Inorganic Chemistry, 13, 2876–2880.

Krieger Lassen, N.C. (1996) The relative precision of crystal orientations measured from electron backscattering patterns. Journal of Microscopy, 181, 72–81.

Lee, D.-C. (2008) ^{182}Hf-^{182}W chronometry and the early evolution history in the acapulcoite-lodranite parent body. Meteoritics and Planetary Science, 43, 675–684.

Livingstone, A. (1980) Johnsomervilleite, a new transition-metal phosphate mineral from the Loch Quoich area, Scotland. Mineralogical Magazine, 43, 833–836.

Mattievich, E. and Danon, J. (1977) Hydrothermal synthesis and Mössbauer studies of ferrous phosphates of the homologous series $Fe_3^{2+}(PO_4)_2(H_2O)_n$. Journal of Inorganic and Nuclear Chemistry, 39, 569–580.

McBride, K. and Mason, B. (1997) GRA 95209: Macroscopic and thin section (,7) description. Antarctic Meteorite Newsletter, 20(1), 9.

McCoy, T.J. and Carlson, W.D. (1998) Opaque minerals in the GRA 95209 lodranite: a snapshot of metal segregation. 29th Annual Lunar and Planetary Science Conference, Houston, Texas, abstract 1675.

McCoy, T.J., Steele, I.M., Keil, K., Leonard, B.F., and Endreß, M. (1994) Chladnite, $Na_2CaMg_7(PO_4)_6$: A new mineral from the Carlton (IIICD) iron meteorite. American Mineralogist, 79, 375–380.

McCoy, T.J., Keil, K, Clayton, R.N., Mayeda, T.K., Bogard, D.D., Garrison, D.H., Huss, G.R., Hutcheon, I.D., and Weiler, R. (1996) A petrologic, chemical, and isotopic study of Monument Draw and comparison with other acapulcoites: Evidence for formation by incipient partial melting. Geochimica et Cosmochimica Acta, 60, 2681–2708.

McCoy, T.J., Keil, K., Clayton, R.N., Mayeda, T.K., Bogard, D.D., Garrison, D.H., and Weiler, R. (1997a) A petrologic and isotopic study of lodranites: Evidence for early formation as partial melt residues from heterogeneous precursors. Geochimica et Cosmochimica Acta, 61, 623–637.

McCoy, T.J., Keil, K., Muenow, D.W., and Wilson, L. (1997b) Partial melting and melt migration in the acapulcoite-lodranite parent body. Geochimica et Cosmochimica Acta, 61, 639–650.

McCoy, T.J., Carson, W.D., Nittler, L.R., Stroud, R.M., Bogard, D.D., and Garrison, D.H. (2006) Graves Nunataks 95209: A snapshot of metal segregation and core formation. Geochimica et Cosmochimica Acta, 70, 516–531.

Merlet, C. (1994) An accurate computer correction program for quantitative electron-probe microanalysis. Mikrochimica Acta, 114, 363–376.

Mittlefehldt, D.W. and Lindstrom, M.M. (1998) Petrology and geochemistry of lodranite Graves Nunataks 95209. Meteoritics and Planetary Science, 33, A111 (abstract).

Mittlefehldt, D.W., Lindstrom, M.M., Bogard, D.D., Garrison, D.H., and Field, S.W. (1996) Acapulco- and Lodran-like achondrites: Petrology, geochemistry, chronology, and origin. Geochimica et Cosmochimica Acta, 60, 867–882.

Modaressi, A., Kaell, J.C., Malaman, B., Gérardin, R., and Gleitzer, C. (1983) Étude du système Fe-P-O (pour $Fe/P \geq 1$) et d'une famille: les oxyphosphates de fer. Materials Research Bulletin, 18, 101–109.

Moore, P.B. (1972) Sarcopside: Its atomic arrangement. American Mineralogist, 57, 24–35.

Nord, A.G. and Ericsson, T. (1982a) The cation distribution in synthetic $(Fe,Mn)_3(PO_4)_2$ graftonite-type solid solutions. American Mineralogist, 67, 826–832.

——— (1982b) Cation distributions in $(Fe_{1-z}Me_z)_3(PO_4)_2$ graftonite-type solid solutions determined by Mössbauer spectroscopy. Zeitschrift für Kristallographie, 161, 209–224.

Nord, A.G. and Kierkegaard, P. (1968) The crystal structure of $Mg_3(PO_4)_2$. Acta Chemica Scandinavica, 22, 1466–1474.

Nord, A.G. and Stephanidis, T. (1980) The cation distribution between five- and six-coordinated sites in some $(Mg,Me)_3(PO_4)_2$ solid solutions. Material Research Bulletin, 15, 1183–1191.

Olsen, E. and Fredriksson, K. (1966) Phosphates in iron and pallasite meteorites. Geochimica et Cosmochimica Acta, 30, 459–470.

Olsen, E.J., Kracher, A., Davis, A.M., Steele, I.M., Hutcheon, I.D., and Bunch, T.E. (1999) The phosphates of IIIAB iron meteorites. Meteoritics and Planetary Science, 34, 285–300.

Patzer, A., Hill, D.H., and Boynton, W.V. (2004) Evolution and classification of acapulcoites and lodranites from a chemical point of view. Meteoritics and Planetary Science, 39, 61–85.

Pellas, P., Fiéni, C., Trieloff, M., and Jessberger, E.K. (1997) The cooling history of the Acapulco meteorite as recorded by the ^{244}Pu and ^{40}Ar-^{39}Ar chronometers. Geochimica et Cosmochimica Acta, 61, 3477–3501.

Prior, D.J., Boyle, A.P., Brenker, F., Cheadle, M.C., Day, A., Lopez, G., Peruzzo, L., Potts, G.J., Reddy, S., Spiess, R., Timms, N.E., Trimby, P.W., Wheeler, J., and Zetterström, L. (1999) The application of electron backscatter diffraction and orientation contrast imaging in the SEM to textural problems in rocks. American Mineralogist, 84, 1741–1759.

Roda, E., Pesquera, A., Fontan, F., and Keller, P. (2004) Phosphate mineral associations in the Cañada pegmatite (Salamanca, Spain): Paragenetic relationships, chemical compositions, and implications for pegmatite evolution. American Mineralogist, 89, 110–125.

Schmid-Beurmann, P. (2001) Stability properties and phase relations of $Fe^{3+}_{4-x}Fe^{3+}_{3x}(PO_4)_3(OH)_{3-3x}O_{3x}$ in the quaternary system $FeO–Fe_2O_3–P_2O_5–H_2O$. Journal of Materials Chemistry, 11, 660–667.

Schmidt, N.-H. and Olesen, N.Ø. (1989) Computer-aided determination of crystal-lattice orientation from electron-channeling patterns in the SEM. Canadian Mineralogist, 27, 15–22.

Škoda, R., Staněk, J., and Čopjaková, R. (2007) Mineral assemblages of the phosphate nodules from the granitic pegmatite at Cyrilov near Velké Meziříčí, Moldanubikum; Part 1—primary and exsolution phases. Acta Musei Moraviae—Scientiae Geologicae, 92, 59–74 (in Czech).

Stöffler, D., Keil, K., and Scott, E.R.D. (1991) Shock metamorphism of ordinary chondrites. Geochimica et Cosmochimica Acta, 55, 3845–3867.

Sugiura, N. and Hoshino, H. (2003) Mn-Cr chronology of five IIIAB iron meteorites. Meteoritics and Planetary Science, 38, 117–143.

Trömel, G. and Schwerdtfeger, K. (1963) Untersuchungen im system Eisen–Phosphor–Sauerstoff. Archiv für das Eisenhüttenwesen, 34, 55–59.

Warner, J.K., Cheetham, A.K., Nord, A.G., von Dreele, R.B., and Yethiraj, M. (1992) Magnetic structure of iron (II) phosphate, sarcopside, $Fe_3(PO_4)_2$. Journal of Materials Chemistry, 2, 191–196.

Zipfel, J., Palme, H., Kennedy, A.K., and Hutcheon, I.D. (1995) Chemical composition and origin of the Acapulco meteorite. Geochimica et Cosmochimica Acta, 59, 3607–3627.

Manuscript received November 20, 2008
Manuscript accepted September 29, 2009
Manuscript handled by Rhian Jones